2001

Modeling Lithium Intercalation in a Porous Carbon Electrode

Gerardine G. Botte

Ralph E. White
University of South Carolina - Columbia, white@cec.sc.edu

Publication Info

Published in *Journal of the Electrochemical Society*, Volume 148, Issue 1, 2001, pages A54-A56.

Journal of The Electrochemical Society, **148** (1) A54-A66 (2001)
S0013-4651/2001/148(1)/A54/13/$7.00 © The Electrochemical Society, Inc.

Modeling Lithium Intercalation in a Porous Carbon Electrode

Gerardine G. Botte* and Ralph E. White,z**

Center for Electrochemical Engineering, Department of Chemical Engineering, University of South Carolina, Columbia, South Carolina 29208, USA

Two different approaches were used to model the insertion of lithium ions into a carbon particle. In the first approach, a concentration gradient was considered as the driving force (DFM) for diffusion while in the second approach chemical potential driving force was used (CPM). Lithium ion-lithium ion interactions are included in the CPM model but not in the DFM model. These approaches were used to model a lithium foil/1 M $LiClO_4$-propylene carbonate/carbon fiber cell. The model predictions indicate that the lithium ion-lithium ion interactions inside the particle play a significant role in predicting the electrochemical and thermal performance of the cell.

Manuscript submitted April 4, 2000; revised manuscript received August 25, 2000.

The intercalation/deintercalation of lithium ions into a carbon particle in the electrode[1] has been modeled as a solid diffusion process by many authors.[2-21] A constant solid diffusion coefficient has been assumed to make the model more efficient,[2-21] even though it has been reported to be a strong concentration dependence.[22,23] This approach consists of solving the diffusion equation in a particle. Assuming that the particle is cylindrical, that the ratio of length to radius is large, and that the electronic resistance within the particle is insignificant, the concentration of lithium inside the particle has a radial variation, and it can be modeled using Fick's second law

$$\frac{\partial y}{\partial \tau} = \frac{1}{R}\frac{\partial}{\partial R}\left(R\frac{\partial y}{\partial R}\right) \quad [1]$$

$$y = y_0 \text{ at } \tau = 0 \;\forall\; R \quad [2]$$

$$\frac{\partial y}{\partial R} = 0 \text{ at } R = 0 \forall\ \tau > 0 \quad [3]$$

$$\frac{\partial y}{\partial R} = -\frac{j_n^+}{D_s}\frac{R_s}{C_{s,max}} \text{ at } R = 1 \forall\ \tau > 0 \quad [4]$$

where $\tau = tD_s/R_s^2$, $y = C_s/C_{s,max}$, and $R = r/R_s$ are dimensionless variables. D_s is the diffusion coefficient in the solid phase, and it is assumed to be constant (this assumption is valid when the concentration of lithium tends to zero), C_s represents the concentration of lithium ions inside the particle, R_s is the radius of the particle, $C_{s,max}$ is the maximum concentration of lithium ions inside the particle, and j_n^+ represents the flux of lithium ions at the surface of the particle. We have called the approach that models the insertion of lithium as a diffusion process given by the solution of Eq. 1-4 the diffusion model (DFM).

On the other hand, Verbrugge and Koch[24] extended the above by using the gradient of the chemical potential of the inserted lithium ions as the driving force, instead of the gradient of the concentration.[1] Assuming the chemical potential as the driving force for the insertion process inside a cylindrical particle[24]

$$\frac{\partial y}{\partial \tau} = \frac{1}{R}\frac{\partial}{\partial R}\left[R\left(1 + \frac{d\ \ln\ \gamma_+}{d\ \ln\ y}\right)\frac{\partial y}{\partial R}\right] \quad [5]$$

The initial condition and the boundary condition at $R = 0$ are given by Eq. 2 and 3, respectively. The other boundary condition is given by

$$\frac{\partial y}{\partial R} = -\frac{j_n^+}{D_s}\frac{R_s}{C_{s,max}\left(1 + \dfrac{d\ \ln\ \gamma_+}{d\ \ln\ y}\right)} \text{ at } R = 1 \forall\ \tau > 0 \quad [6]$$

The quantity $(1 + d \ln \gamma_+/d \ln y)$ represents the lithium ion-lithium ion interactions inside the particle or the activity coefficient term in the solid phase. Verbrugge and Koch showed that this quantity is a strong function of concentration,[24] and it could not be neglected even to obtain qualitative agreement with experimental data in a partially graphitic carbon fiber when it is charged and/or discharged potentionstatically. We have called this approach the chemical potential model (CPM).

Both models assume a constant solid diffusion coefficient at the dilute state. The difference between the two approaches is that the CPM accounts for the effect of the activity coefficients in the solid phase, while the DFM does not. The CPM is more realistic than the DFM. However, its use in the modeling of a lithium cell is less efficient than the DFM because its implementation means solving at least a pseudo-two-dimensional model (*i.e.*, the case of a one-dimensional cell and the radial dimension of a particle, as we show later). The DFM is more efficient because integration in the radial dimension of a particle can be accomplished by using Duhamel's superposition theorem,[7,11,14,15,17,19-21,25-27] transforming a pseudo-two-dimensional model in a one-dimensional model, as we show later. The objective of this paper is to compare the predictions of the two models, DFM and CPM, for the performance of a lithium foil cell under normal and abusive conditions (high discharge rates). We have compared both approaches in some limiting cases and/or simplified models (potentiostatic charge/discharge of a particle carbon fiber and galvanostatic discharge of a lithium foil cell under diffusion limitations) and into a lithium foil cell during a galvanostatic discharge. We have developed a pseudo-two-dimensional model that uses concentrated solution theory framework[28] to simulate the behavior of a lithium foil cell.

Limiting Cases and Simplified Models

We have developed two mathematical models (DFM and CPM) to simulate the potentiostatic charge/discharge of a partially graphitic carbon fiber (Fortafil),[24] and the galvanostatic discharge of a lithium foil cell under solid diffusion limitations. In both cases, 1 M $LiClO_4$ in propylene carbonate (PC) was used as the electrolyte. Figure 1 shows a schematic representation of the carbon fiber. The electrochemical reaction on the surface of the carbon fiber is given by[24]

$$Li^+ + e^- + \theta_s \underset{k_a}{\overset{k_c}{\rightleftharpoons}} [Li^{+\delta} - \theta_s^{-\delta}] \quad [7]$$

where δ represents the lithium charge. It has been proved by X-ray photoelectron spectroscopy (XPS) that after insertion the lithium

* Electrochemical Society Student Member.
** Electrochemical Society Fellow.
z E-mail: rew@sc.edu

still retains a fraction of the positive charge (+δ), and the carbon sites take a negative charge of equal magnitude (−δ).[29] During the charge of the carbon fiber, the lithium ions are intercalated into the carbon particle and vice versa. We used the same equations developed by Verbrugge and Koch[24] for the dependence of the activity coefficient on the intercalation fraction

$$f_2 = 1 + \frac{d \ln \gamma_+}{d \ln y} = 1 + \sum_{k=2}^{7} \frac{\Omega_k}{\Re T} k(k-1)\left(y^{k-1} - y^k\right) \quad [8]$$

The open-circuit potential of the carbon fiber *vs*. a lithium reference electrode is given by[24]

$$U = U_s + \frac{\Re T}{F} \ln\left(\frac{1 - y|_{R=1}}{y|_{R=1}}\right) - \frac{1}{F}\sum_{k=2}^{7} \Omega_k k \left(y|_{R=1}\right)^{k-1}$$

$$\text{for } 0 < y|_{R=1} < 0.985 \quad [9]$$

where U represents the open-circuit cell potential with respect to a metallic lithium electrode, U_s is the standard cell potential (infinitely dilute solution of $Li^{+\delta}$ in the carbon fiber) with respect to a metallic lithium electrode, and Ω_k are the self-interaction energies.

Figure 2a presents the dependence of the activity coefficient (f_2, left side of Eq. 8) and the open-circuit potential *vs*. the lithium intercalation fraction. The factor f_2 varies significantly with the lithium intercalation fraction, changes of up to one order of magnitude can be observed in Fig. 2a. At low lithium intercalation fractions ($y < 0.2$), f_2 increases with increasing the lithium ion concentration due to repulsive effects (thus enhancing the diffusion inside the particle). At $y = 0.2$, f_2 becomes the maximum value for diffusion, where the repulsive effects are very significant. At higher lithium intercalation fractions ($y > 0.2$), f_2 decreases with increasing the lithium ion concentration due to steric effects (*i.e.*, low mobility due to large lithium ion concentrations). The open-circuit potential varies from $U \approx 1.11$ V ($y|_{R=1} \approx 0.0$) for the discharged state up to $U \approx 0.0$ V ($y|_{R=1} \approx 0.985$) for the charged state of the carbon fiber. The open-circuit potential does not show any plateaus or phase changes because the carbon fiber used is not a well-ordered material.[24] The open-circuit potential is very steep at low states of charge (see Fig. 2b).

The flux of lithium ions at the surface of the particle is equal to the electrochemical reaction rate per unit of surface area of the particle as given by a Butler-Volmer reaction rate expression[24]

$$j_n^+ = K\left(C\left[1 - y|_{R=1}\right]\right)^{1-\beta}\left(y|_{R=1}\right)^{\beta}\left\{\exp\left[\frac{(1-\beta)F}{\Re T}(V-U)\right] - \exp\left[\frac{-\beta F}{\Re T}(V-U)\right]\right\} \quad [10]$$

where C is the concentration of the electrolyte and K is the reaction rate constant ($K = k_c^{1-\beta} k_a^{\beta}$). The values used for the standard cell potential, the self-interaction energies, and the kinetic parameters are shown in Table I. The open-circuit potential is evaluated at the surface of the particle where the electrochemical reaction (Eq. 7) takes place.

Carbon fiber model under potential dynamic control.—The equations for the performance of the particle under potential dynamic control are given by Eq. 1-4 for the DFM approach and Eq. 2, 3, 5, 6 for the CPM approach. These equations were discretized by using the implicit method for the temporal dimension and three-point finite difference formulas for both the first and second derivatives in the radial dimension in the particle. The resulting coupled

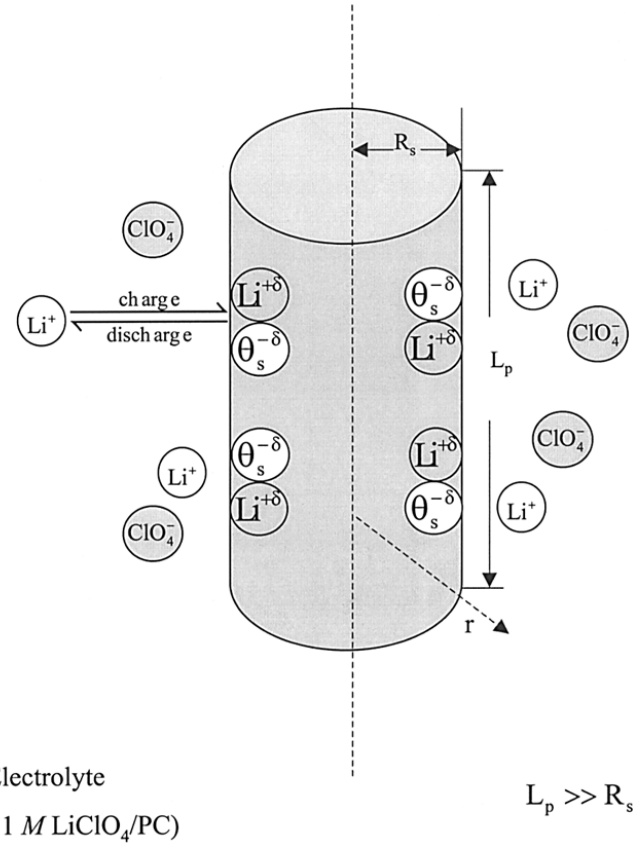

Figure 1. Schematic representation of the carbon fiber. When the particle is charged lithium ions are intercalated ($Li^{+\delta}$, see Eq. 7) at the surface of the particle and they diffuse inside the particle. The opposite process takes place during discharge.

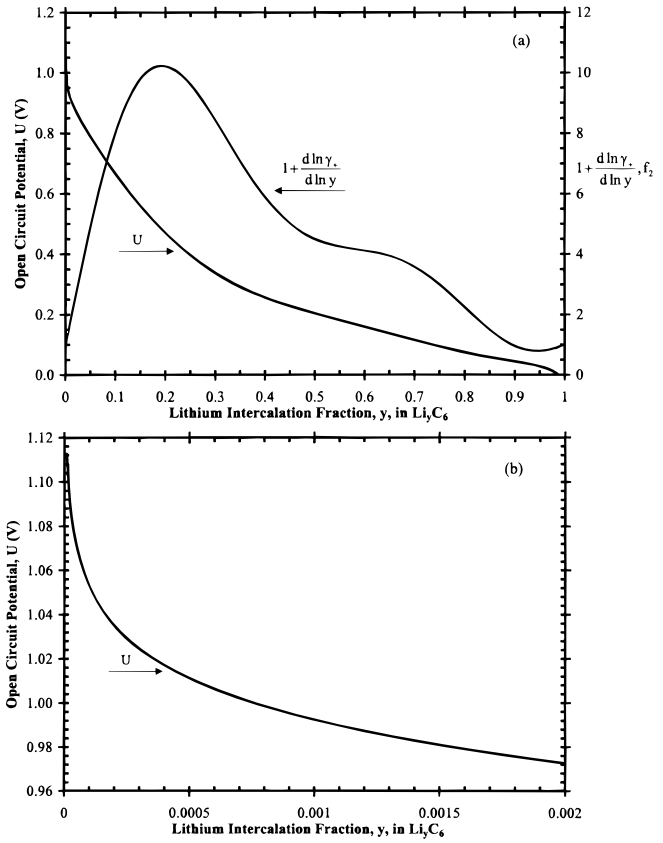

Figure 2. Open-circuit potential and activity coefficients *vs*. lithium intercalation fraction. (a) In the whole range of lithium intercalation fractions. (b) At small lithium intercalation fractions.

Table I. Standard cell potential, interaction energies, and kinetic parameters for the carbon electrode.

Parameter	Value[a]
U_s [b]	0.8170 V
Ω_2/F	0.9926 V
Ω_3/F	0.8981 V
Ω_4/F	−5.630 V
Ω_5/F	8.585 V
Ω_6/F	−5.784 V
Ω_7/F	1.468 V
$C_{s,max}$	18,000 mol/m^3
β	0.5
K	3.28×10^{-6} mol$^{1/2}$/m$^{1/2}$ s

[a] Data obtained from Ref. 24.
[b] Evaluated at infinitely dilute conditions.[24]

nonlinear algebraic equations were solved by using the Band(J) algorithm.[28] In this case the pore wall flux for both approaches is obtained by Eq. 10. The particle is assumed to be immersed in an excess of electrolyte, therefore, the concentration of the electrolyte at the surface of the particle was assumed constant ($C = 1$ M).

The performance of the particle was evaluated at $T = 25$°C. The problem was further simplified by assuming that the potential of the solid particle is uniform and equal to the applied potential (U_{app}). Under potentiodynamic control, the applied potential changes linearly with time and is given by[30]

$$U_{app} = U_0 + \nu f_1 t \quad [11]$$

where U_0 is the initial applied potential, ν is the sweep rate, and f_1 is a conversion factor. At the initial time, the initial applied potential was assigned to be the open-circuit potential at the initial lithium-ion intercalation fraction.

The current density at the surface of the particle (i) can be calculated by

$$i = Fj_n^+ \quad [12]$$

Figure 3 shows the potentiostatic charge/discharge of a carbon fiber particle in 1 M $LiClO_4$/PC. Figure 3a shows a voltammogram for a scan rate of 10 mV/s. The voltammogram was obtained as follows: 1, the carbon particle was charged from its initial state ($y_0 = 0.01$, $U_0 = 0.91489$ V, and $i = 0.0$ A/m^2) to 0.075 V at a sweep rate of $\nu = -10$ mV/s. 2, The carbon particle was then discharged to 1.5 V at a sweep rate of $\nu = 10$ mV/s. 3, The particle was again charged to 0.075 V at a sweep rate of $\nu = -10$ mV/s. 4, Steps 2 and 3 were repeated (cycling from 0.075 to 1.5 V and vice versa) until the periodic state was reached. The periodic state is the state, at which the results are uniform and sustained during consecutive cycles, when cycled under the same conditions (sweep rate and minimum and maximum applied potentials). The periodic state was reached in cycle 3 for both the CPM and the DFM. Figure 3 reproduces the results obtained previously by Verbrugge and Koch.[24]

Figure 3a shows that there are significant differences in the shape of the voltammograms obtained with the CPM model and the DFM model. The results obtained with our model for the CPM approach match very well the results reported by Verbrugge and Koch.[24] The differences in the shapes of the voltammograms for the CPM and DFM approaches are due to the lithium ion-lithium ion interactions inside the particle, and they can be understood by analyzing the results shown in Fig. 3b and c.

Figures 3b and c present the variation of the lithium ion intercalation fraction in the radial direction of the particle at 0.075, and 1.5 V, respectively. It can be noticed that at the lowest potential (0.075 V) intercalation into the particle takes place while at the highest potential (1.5 V) deintercalation from the particle takes place. In both figures (3b and c), significant differences in the concentration profiles were observed between the CPM and the DFM approaches. In the DFM approach the diffusion limitations are more significant compared to the CPM approach leading to abrupt changes in concentration profiles. At 0.075 V the lithium ion intercalation fraction at the surface of the particle is about 0.58 (see Fig. 3b), and the corresponding value of the activity coefficient is about $f_2 = 4$ (see Fig. 2a). Therefore, the overall solid diffusion coefficient (product of D_s by f_2) in the CPM is four times larger than the one used for the DFM approach at the surface of the particle. A larger overall solid diffusion coefficient makes the pore flux at the surface of the particle larger for the CPM than for the DFM (see Eq. 6 and 4), generating a larger cathodic current (see Eq. 12) in the CPM as shown in

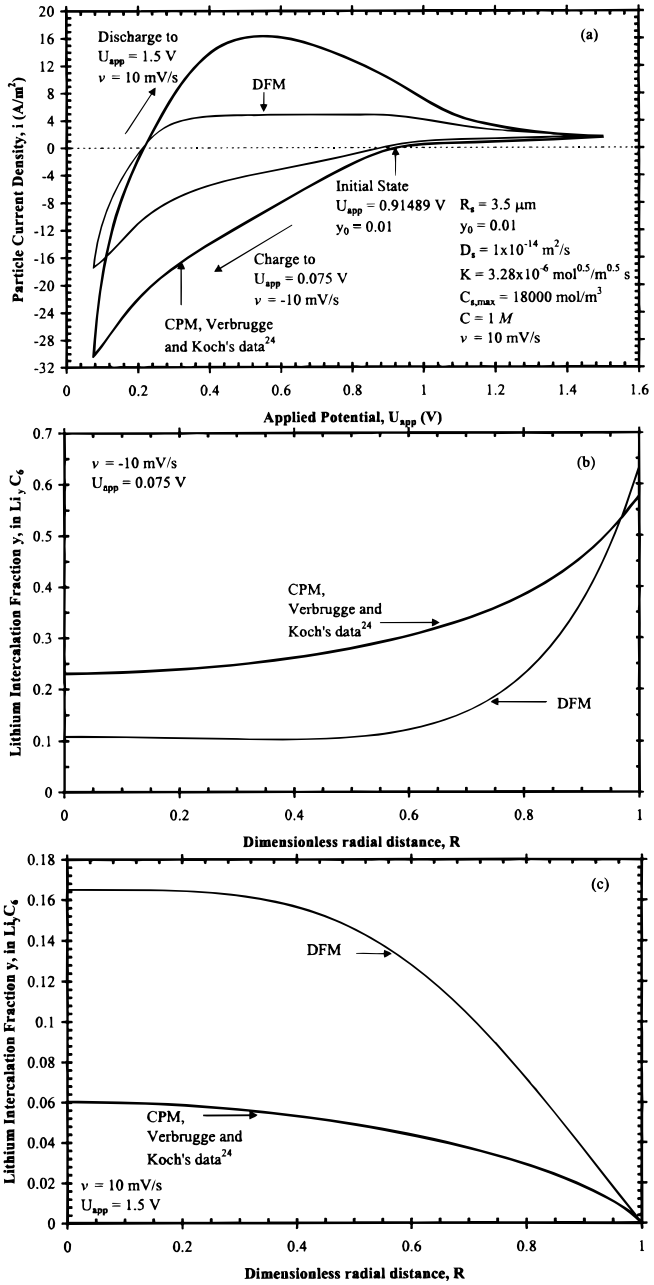

Figure 3. Potentiostatic discharge of a carbon fiber particle in 1 M $LiClO_4$/PC. The temperature of the particle was kept constant at 25°C. The concentration of the electrolyte was assumed to be constant (1 M). (a) Voltammogram for a scan rate of 10 mV/s. (b) Lithium intercalation fraction inside the particle at the end of the charge ($U_{app} = 0.075$ V). (c) Lithium intercalation fraction inside the particle at the end of the discharge ($U_{app} = 1.5$ V).

Fig. 3a. At 1.5 V the concentration at the surface of the particle using the CPM approach is very close to zero. The value of the activity coefficient (shown in Fig. 2) for the CPM will be 1.0, making the current obtained for the CPM and the DFM the same as shown in Fig. 3c (see Eq. 6 and 4). The maximum anodic current obtained by the CPM is larger than the one obtained by the DFM (see Fig. 3a) due to the lithium ion-lithium ion interactions, that is, excluding the interactions makes the diffusion limitations stronger.

Finally, it is worth mentioning that voltammograms of microelectrodes have been used to determine diffusion coefficients and kinetics constants for the electrochemical reactions.[24,30] Therefore, since the results of the voltammogram obtained with the DFM approach do not match the experimental data (see Fig. 3a), any diffusion coefficient or kinetic constant values obtained by using the DFM approach might not represent the real parameters for the system.

Solid diffusion limitations in a lithium foil cell (simplified model of the cell).—Doyle *et al.*[11] have demonstrated the importance of diffusion in the solid phase in a cell using the dimensionless parameter S_c. This parameter represents the ratio of the diffusion time to the discharge time of a given cell, and can be expressed by[11]

$$S_c = \frac{R_s^2 i_{app}}{D_s F(1-\epsilon_1) C_{s,max} L_1} \quad [13]$$

where i_{app} is the applied current density of the cell, ϵ_1 and L_1 are the porosity and the thickness of the electrode of which diffusion limitation effects are being evaluated, respectively. When diffusion limitations in the electrode under consideration are significantly limiting the electrochemical performance of the cell, the parameter $S_c >> 1$.[11]

The electrochemical performance of a cell that is charged and/or discharged galvanostatically, and operating under solid diffusion limitations can be modeled using a simple model.[3] This means that we can have an approximation of the electrochemical performance of the cell without solving more completed and complicated equations, as we show in the next section. We use the approximate model proposed by Doyle and Newman[3] to study the galvanostatic discharge of a lithium foil cell (that consists of carbon fiber electrode, separator, electrolyte, and lithium foil electrode; more details of the cell are given later) that operates under solid diffusion limitations ($S_c >> 1$). The essence of the approximate model is that modeling the performance of one particle in the electrode can approximate the performance of the cell. Other assumptions of the model are (*i*) one porous electrode in the cell, (*ii*) a uniform concentration of the electrolyte over the time of discharge of the cell, (*iii*) a reversible charge-transfer process, and (*iv*) a uniform reaction distribution in the porous electrode (equal to its average value). It is worth mentioning that during discharge of the cell lithium ions are dissolved from the lithium foil electrode and intercalated into the carbon fiber electrode. With all these assumptions, the average pore wall flux in the carbon electrode can be approximated by[3]

$$j_n^+ = \frac{i_{app}}{aFL_1} \quad [14]$$

where *a* (see Eq. A-8) is the interfacial area of solid-phase particles per unit volume of porous electrode. The equations for the performance of the cell can be simplified and its performance can be described by the solution of Eq. 1-4 for the DFM approach and Eq. 2, 3, 5, 6 for the CPM approach. Thus the material balance in one particle can be extrapolated to evaluate the performance of the electrode by using the total pore wall flux of the electrode (see Eq. 14) instead of the flux of one particle. Equations 1-4 and Eq. 2, 3, 5, 6 were discretized by using the implicit method for the temporal dimension and three-point finite difference formulas for both the first and second derivatives in the radial dimension. The resulting coupled nonlinear algebraic equations were solved by using the Band(J) algorithm.[28]

Neglecting the ohmic resistance of the separator, the potential of the cell can be obtained by solving Eq. 10. The potential (*V*) can be obtained from this equation by using Maple V. The solution of the equation gives two roots (one real and one imaginary). The root that makes physical sense was used to evaluate the potential of the cell and is given by (fixing $\beta = 0.5$)

$$V = U + 2\frac{RT}{F}\ln\left[\frac{1}{2}\frac{-\sqrt{1-y|_{R=1}}\sqrt{y|_{R=1}}j_n^+ - \sqrt{\text{Number}}}{-CKy|_{R=1} + CK\left(y|_{R=1}\right)^2}\right]$$

$$\text{Number} = y|_{R=1}j_n^{+2} - (y|_{R=1}j_n^+)^2 + 4(CKy|_{R=1})^2 - 8C^2K^2(y|_{R=1})^3 + 4C^2K^2(y|_{R=1})^4 \quad [15]$$

Figure 4 shows the galvanostatic discharge of a lithium foil/carbon fiber electrode cell after $t = 10$ min. The applied current density was $i_{app} = 180.69$ A/m^2 equivalent to 3C (the theoretical discharge rate of the cell is 1C = 60.23 A/m^2 for $C_{s,max} = 18{,}000$ mol/m^3, this value can be calculated from Eq. A-12). The electrolyte concentration was assumed constant ($C = 1$ M). The cell was assumed to operate under solid diffusion limitations, $S_c = 1.57$. Figure 4a presents the cell potential *vs*. the average lithium intercalation fraction in the cell (y_{avg}). The average lithium intercalation fraction in the cell will be the same as the average intercalation in the particle (only one particle is used in the model), and is given by

$$y_{avg} = 2\int_{R=0}^{R=1} yRdR \quad [16]$$

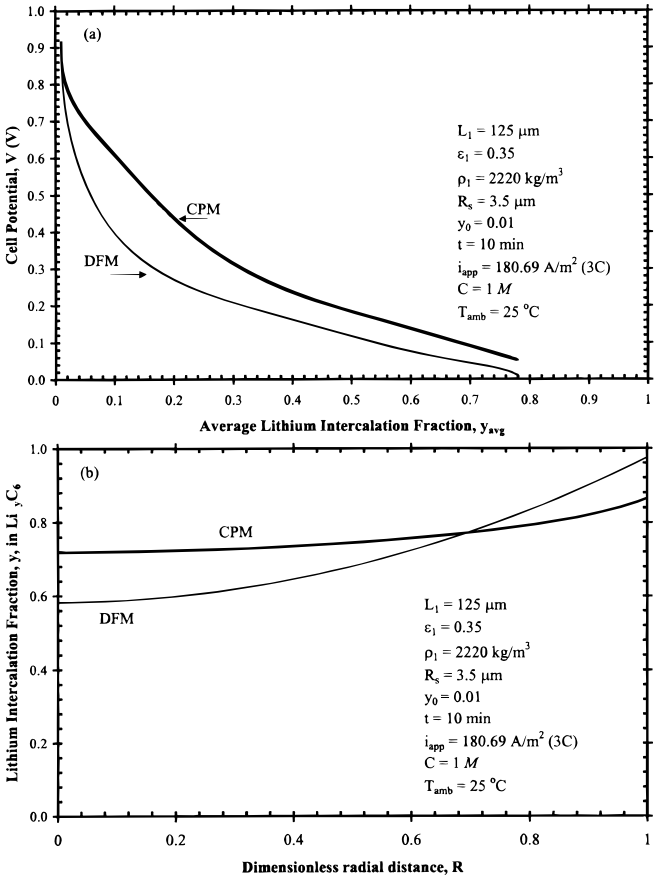

Figure 4. Galvanostatic discharge at $i_{app} = 180.69$ A/m^2 (3C) of a lithium foil/carbon fiber electrode cell with 1 M $LiClO_4$/PC electrolyte under solid-phase diffusion limitations (simplified model) during $t = 10$ min. The temperature of the cell was kept constant at 25°C. (a) Cell potential *vs*. average lithium intercalation fraction in the cell. (b) Lithium intercalation fraction *vs*. radial distance at the end of the carbon electrode ($L_1 = 125$ μm).

Figure 4a shows significant differences between the CPM and the DFM approaches. The differences are due to the lithium ion-lithium ion interactions inside the particle. By neglecting the effect of these interactions inside the particle, the diffusion limitations inside the particle become stronger, because the activity coefficient term is not included. The effect of the diffusion limitations inside the particle can be seen in Fig. 4b. This figure shows the lithium intercalation fraction inside the particle *vs*. the radius of the particle (at the end of the electrode L_1). As mentioned before, during discharge of the cell lithium ions are intercalated into the carbon fiber. The profile shown by the DFM approach indicates stronger diffusion limitations than the one shown by the CPM approach (the concentration of lithium ion is more uniformly distributed in the CPM than in the DFM).

We have observed significant differences between the DFM and the CPM for the limiting and simplified cases studied alone. The differences observed justify the evaluation of the two different approaches in a more complicated system such as a lithium foil cell. This system includes the effect of the separator and the variation of the electrolyte concentration in the cell, where more realistic results can be obtained than when using the solid diffusion limitation model.

Lithium Foil Cell Model

We modeled the galvanostatic discharge behavior of the Li/Li_yC_6 cell sandwich shown in Fig. 5. This is a pseudo two-dimensional model with transport of lithium ions across the cell and within the solid-phase particles, which are assumed to be cylindrical with $L_p >> R_s$. Since the length of the particles was assumed to be much larger than the radius, transport of inserted lithium ions needs to be considered only in the radial direction in a particle. To avoid complexity, volume changes associated with electrode expansion and contraction during cycling were ignored.

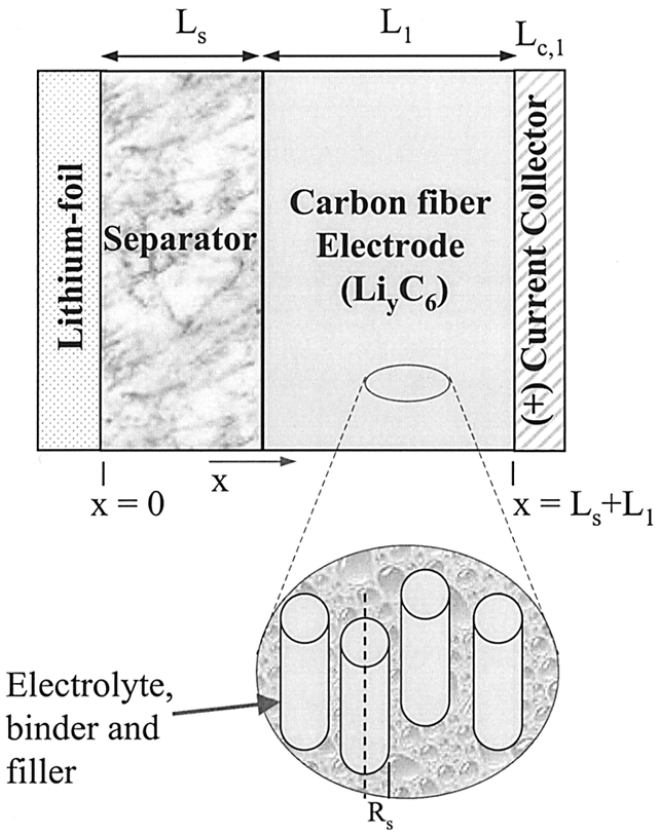

Figure 5. Idealized schematic diagram of the lithium foil cell. Cell sandwich consists of lithium foil, separator, and carbon fiber electrode. The active material is depicted and modeled as cylindrical particles ($L_p >> R_s$). During the discharge of the cell lithium ions are disolved from the lithium foil electrode and intercalated into the carbon fiber electrode.

The cell consists of a lithium foil negative electrode, a microporous polyethylene separator, and a carbon fiber positive electrode. The electrolyte used was lithium perchlorate salt with propylene carbonate solvent (1 M $LiClO_4$/PC). The carbon fiber was chosen because there is data available[24] to perform the comparison between the DFM and the CPM (the self-interaction parameters are known). During the discharge of the cell, lithium is dissolved into lithium ions from the negative electrode, followed by diffusion and migration through the separator and finally intercalation into the positive electrode. The model includes two regions as shown in Fig. 5. An approximate concentrated solution theory framework[28] was used to model the transport of lithium ions through the cell. In the solution phase of the carbon electrode, the equations are given by[25]

$$\epsilon_k \frac{\partial C}{\partial t} = \frac{\partial}{\partial x}\left(\epsilon_k D_{\text{eff},k} \frac{\partial C}{\partial x}\right) - \frac{i_2}{F}\frac{\partial t_+^0}{\partial x} + a j_n^+ (1 - t_+^0) \qquad k = 1, s \quad [17]$$

The potential in the solution phase is[25]

$$\frac{\partial \phi_2}{\partial x} = \frac{-i_2}{\kappa_{\text{eff},k}} + \frac{\mathcal{R}T}{F}(1 - t_+^0)\frac{1}{C}\frac{\partial C}{\partial x} \qquad k = 1, s \quad [18]$$

The solution-phase potential (ϕ_2) is defined with respect to a lithium reference electrode. The flux of lithium ions across the solid-liquid interface is given by[28]

$$a j_n^+ = \frac{1}{F}\frac{\partial i_2}{\partial x} \quad [19]$$

The potential in the solid phase of the electrode is given by Ohm's law[28]

$$\frac{\partial \phi_1}{\partial x} = -\frac{(i_{\text{app}} - i_2)}{\sigma_{\text{eff}}} \quad [20]$$

The effective properties used in Eq. 17, 18, and 20 are calculated using Bruggeman's correction (see Appendix).

The insertion of lithium ions into the electrode particles was modeled using two different approaches: DFM and CPM. Equation 1-4 were used for the DFM, and Eq. 2, 3, 5, and 6 were used for the CPM. No film resistance was included in the model, therefore, the pore-wall flux is given by the Butler-Volmer rate expression given by Eq. 10, and the potential is defined by $V = \phi_1 - \phi_2$.

In the separator region the solution-phase current density (i_2) equals the applied current density (i_{app}), because the separator is assumed to be inert. Equations 17 and 18 are used in the separator (*i.e.*, $k = s$). The pore-wall flux in this region is zero. The initial condition used for the solution of Eq. 17 is

$$C = C_0 \text{ at } t = 0 \;\forall\; x \quad [21]$$

The material balance equation (Eq. 17) is second order with respect to its derivatives; therefore two boundary conditions are needed

$$N_+ = \frac{i_{\text{app}}}{F} \text{ at } x = 0 \;\forall\; t > 0 \quad [22]$$

$$N_+ = 0 \text{ at } x = L_s + L_1 \;\forall\; t > 0 \quad [23]$$

The reaction at the lithium electrode surface ($x = 0$) is given as

$$Li \rightleftharpoons Li^+ + e^- \quad [24]$$

The kinetic expression is given by[25]

$$i_{\text{app}} = F K_{\text{Li}} C^{0.5}\left\{\exp\left[\frac{\alpha F(\phi_1 - \phi_2)}{\mathcal{R}T}\right] - \exp\left[\frac{-(1-\alpha)F(\phi_1 - \phi_2)}{\mathcal{R}T}\right]\right\} \quad [25]$$

Table II. Summary of model equations.

Region	Variable	Equation
$x = 0$	y	$y = 0\ \forall\ R,\ 0 \le R \le 1$ DFM and CPM
	C	$N_+ = \dfrac{i_{app}}{F}$
	i_2	$i_2 = i_{app}$
	η	$\dfrac{\partial \eta}{\partial x} = \dfrac{i_2}{\kappa_{eff,s}} - \dfrac{\Re T}{F}\dfrac{(1-t_+^0)}{C}\dfrac{\partial C}{\partial x}$
$0 < x < L_s$ Separator	y	$y = 0\ \forall\ R,\ 0 \le R \le 1$ DFM and CPM
	C	$\epsilon_s \dfrac{\partial C}{\partial t} = \dfrac{\partial}{\partial x}\left(\epsilon_s D_{eff,s}\dfrac{\partial C}{\partial x}\right) - \dfrac{i_2}{F}\dfrac{\partial t_+^0}{\partial C}\dfrac{\partial C}{\partial x}$
	i_2	$i_2 = i_{app}$
	η	$\dfrac{\partial \eta}{\partial x} = \dfrac{i_2}{\kappa_{eff,s}} - \dfrac{\Re T}{F}\dfrac{(1-t_+^0)}{C}\dfrac{\partial C}{\partial x}$
$x = L_s$ Separator-composite electrode interface	y	DFM: Eq. 1-3 $0 \le R < 1$ $\dfrac{\partial y}{\partial R} = -\dfrac{j_n^+}{D_s}\dfrac{R_s}{C_{s,max}}$ at $R = 1$
		CPM: Eq. 2-3, 5 $0 \le R < 1$ $\dfrac{\partial y}{\partial R} = -\dfrac{j_n^+}{D_s}\dfrac{R_s}{C_{s,max} f_2}$ at $R = 1$
	C	$N_+\big\vert_{x=-L_s} = N_+\big\vert_{x=+L_s}$
	i_2	$i_2 = i_{app}$
	η	$\dfrac{\partial \eta}{\partial x} = \dfrac{-i_{app}}{\sigma_{eff}} + i_2\left(\dfrac{1}{\sigma_{eff}} + \dfrac{1}{\kappa_{eff,1}}\right) - \dfrac{\Re T}{F}\dfrac{(1-t_+^0)}{C}\dfrac{\partial C}{\partial x}$
$L_s < x < L_s + L_1$ Composite Electrode	y	DFM: Eq. 1-3 $0 \le R < 1$ $\dfrac{\partial y}{\partial R} = -\dfrac{j_n^+}{D_s}\dfrac{R_s}{C_{s,max}}$ at $R = 1$
		CPM: Eq. 2-3, 5 $0 \le R < 1$ $\dfrac{\partial y}{\partial R} = -\dfrac{j_n^+}{D_s}\dfrac{R_s}{C_{s,max} f_2}$ at $R = 1$
	C	$\epsilon_1 \dfrac{\partial C}{\partial t} = \dfrac{\partial}{\partial x}\left(\epsilon_1 D_{eff,1}\dfrac{\partial C}{\partial x}\right) - \dfrac{i_2}{F}\dfrac{\partial t_+^0}{\partial x} - a\dfrac{D_s}{R_s}C_{s,max} f_2 \dfrac{\partial y}{\partial R}\Big\vert_{R=1}(1-t_+^0)$
	i_2	$-a\dfrac{D_s}{R_s}C_{s,max} f_2 \dfrac{\partial y}{\partial R}\Big\vert_{R=1} = \dfrac{1}{F}\dfrac{\partial i_2}{\partial x}$
	η	$\dfrac{\partial \eta}{\partial x} = \dfrac{-i_{app}}{\sigma_{eff}} + i_2\left(\dfrac{1}{\sigma_{eff}} + \dfrac{1}{\kappa_{eff,1}}\right) - \dfrac{\Re T}{F}\dfrac{(1-t_+^0)}{C}\dfrac{\partial C}{\partial x}$
$x = L_s + L_1$	y	DFM: Eq. 1-3 $0 \le R < 1$ $-a\dfrac{D_s}{R_s}C_{s,max}\dfrac{\partial y}{\partial R}\Big\vert_{R=1} = \dfrac{1}{F}\dfrac{\partial i_2}{\partial x}$ at $R = 1$
		CPM: Eq. 2-3, 5 $0 \le R < 1$ $-a\dfrac{D_s}{R_s}C_{s,max} f_2 \dfrac{\partial y}{\partial R}\Big\vert_{R=1} = \dfrac{1}{F}\dfrac{\partial i_2}{\partial x}$ at $R = 1$
	C	$N_+ = 0$
	i_2	$i_2 = 0$
	η	$-\dfrac{D_s}{R_s}C_{s,max} f_2 \dfrac{\partial y}{\partial R}\Big\vert_{R=1} = j_n^+$

where: $j_n^+ = K\left(C\left[1 - y\big\vert_{R=1}\right]\right)^{1-\beta}\left(y\big\vert_{R=1}\right)^{\beta}\left\{\exp\left[\dfrac{(1-\beta)F}{\Re T}(\eta - U)\right] - \exp\left[\dfrac{-\beta F}{\Re T}(\eta - U)\right]\right\}$

DFM: $f_2 = 1$

CPM: $f_2 = 1 + \dfrac{d \ln \gamma_+}{d \ln y}$

where K_{Li}, and α are the reaction rate constant, and the transfer coefficient for the lithium deposition-dissolution reaction, respectively.

At the separator-electrode interface ($x = L_s$), the flux and variables are taken to be continuous. To reduce the number of variables, the potentials in the solid-phase and solution-phase were combined

$$\eta = \phi_1 - \phi_2 \quad [26]$$

where η represents the local surface overpotential. Equations 17-20 and 10 were simplified and combined.

Table II shows a summary of the simplified equations used in the model, including the boundary conditions. There are three independent variables (*i.e.*, *t*, *x*, and *R*) and four dependent variables (*i.e.*, *y*, *C*, i_2, and η) at each node in each region of the cell.

The energy balance in the cell was formulated using the procedure by Botte *et al.*,[21] without including the effect of the decomposition reaction of the carbon electrode. The following assumptions were made for the formulation of the energy balance[21]: (*i*) the temperature is uniform throughout the cell at a given instant in time, (*ii*) the heat capacity of the cell is calculated as an average of all the components of the cell, and (*iii*) enthalpy of mixing and phase-change terms were neglected.

Considering the assumptions, the energy balance in the cell is given by[21]

$$\rho C_p \frac{\partial T}{\partial t} = Q + a_1 i_{app}\left(U - T\frac{dU}{dT} - V\right) \quad [27]$$

where ρ is the density of the cell, C_p is the heat capacity of the cell, a_1 represents the geometric electrode surface area per volume of the cell, and Q is the heat release per unit volume of the cell to the ambient by convection. The heat release to the ambient is obtained by[21]

$$Q = a_1 a_2 h\,(T_{amb} - T) \quad [28]$$

where a_2 is the ratio of external cell surface area to geometric electrode surface area, T_{amb} is the ambient temperature, and h is the heat transfer coefficient.

Numerical Technique

The equations shown in Table II were solved using the collapsing technique,[31] to deal with the radial dependence of the equations. The variables were discretized in the *R* and in the *x* directions. Figure 6 presents the discretization of the radial dimension of the particle (*R*) and the thickness of the cell (*x*). All the variables in the *R* direction are collapsed to the *x* direction using the collapsing technique.[31] In this technique, the radial dimension is discretized and collapsed at each node point in the *x* direction as shown in Fig. 6. As we mentioned before the independent variables are *y*, *C*, i_2, and η. But *y* (lithium intercalation fraction) changes depending on the radial position and *x* position, therefore we will have as many values of *y* in a given *x* node as many nodes we used in the radial direction (y_1, y_2, y_3, ..., y_{nr}). 51 nodes were used in the radial direction ($nr = 51$) and the equations were discretized using Taylor's series approximation of $(\Delta R)^2$ order of accuracy. Therefore, the dependent variable *y*, generates 51 dependent variables, that is, 54 equations were solved at each node point in the *x* direction (y_1, y_2, ..., y_{51}, *C*, i_2, and η) simultaneously.

The material balance in the cell was formulated using control volume formulation[32] to insure the conservation of mass in the cell. The concentration of the electrolyte was discretized using the Piece-Wise linear profile.[32]

The implicit method was used for the time dependence. The overpotential (η) was discretized using the two-point forward approximation and the solution-phase current density (i_2) was discretized using the two-point backward approximation to insure the solution of the equations using Band(J) (avoiding the DETERMINAT = 0 problem caused by Band(J) for these type of equations as proposed by Curtis *et al.*[33]). The discretized equations and their jacobians were generated using Maple V.[34] The resulting coupled nonlinear algebraic equations were solved using the subroutine Band(J).[28]

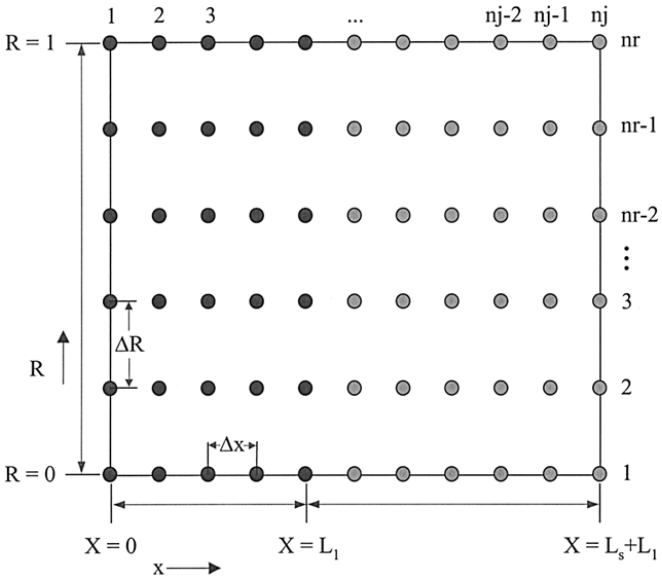

Figure 6. Discretization of the radial dimension of the particle (*R*) and the thickness of the cell (*x*), pseudo-two-dimensional model. The collapsing technique[31] was used for the solution of the problem. Δx, ΔR, *nr*, and *nj* represent the grid size in the *x* direction, the grid size in the *R* direction, the total number of nodes in the *R* direction, and the total number of nodes in the *x* direction, respectively.

Once the solution of the equations shown in Table II is obtained, the temperature in the cell can be evaluated by solving Eq. 27, with the initial condition

$$T = T_0 \text{ at } t = 0 \;\forall\; x \quad [29]$$

All the transport properties required for the system were evaluated at 25°C for the reasons explained by Botte *et al.*[21] An average concentration at the surface of the particle in the whole electrode was used to evaluate the open-circuit potential and the entropy terms (dU/dT) used in Eq. 27. The initial conditions and the transport properties used for the simulation are shown in Table III.

The execution time of the program depends on the conditions of the simulation and the approach used. For instance, it took approximately 3.5 h to simulate the galvanostatic discharge of the cell at 2C to 0.01 V cutoff potential with the DFM using a PC with 128 MB RAM and a 333 MHz Pentium II processor. It took approximately 6.0 h to simulate the same case using the CPM. In all of the cases, the CPM required more computational time than the DFM, not only because of the convergence of the results but also because the predicted discharge time for the cell by the DFM approach is less than that for the CPM approach.

Results and Discussion

The model parameters used for the simulation are given in Table IV. Figure 7 shows the potential of the cell as a function of the utilization of the carbon electrode at different galvanostatic discharge rates. The line with circle symbols represents the open-circuit potential of the cell. The potential of the cell is given by

$$V = \phi_1\big|_{x=L_s+L_1} - \phi_1\big|_{x=0} \quad [30]$$

Equation 30 can be rearranged and defined as a function of the overpotential

$$V = \eta\Big|_{x=0} + \phi_{1,kin} + \int_{x=L_s}^{x=L_s+L_1} -\frac{\left[i_{app} - i_2(x)\right]}{\sigma_{eff}}dx \quad [31]$$

where the contribution to the potential by the reaction at the lithium electrode ($\phi_{1,kin}$) is obtained from Eq. 25. The utilization of the cell is defined by

Table III. Initial conditions of the cell and transport properties.

Variable	Value	Ref.
C_0	1000 mol/m^3	IC
T_0	298 K	IC
y_0	0.01	IC
D	2.6×10^{-10} m^2/s	38
D_s	1.0×10^{-14} m^2/s	24
t_+^0	0.20	38
$\kappa_{\text{eff},k}$ (k = 1, s)	$0.0001 + \epsilon_k^{1.5} C^{0.855}[0.00179e^{[-0.08(0.00083C-0.6616)^2-0.0010733C+0.855]}]$	25
σ	100 S/m	7

IC: initial condition.
1: solid phase.
s: separator.

$$u = \int_{x=L_s}^{x=L_s+L_1} \frac{y_{avg}}{L_1} dx \qquad [32]$$

where the average intercalation fraction inside the particle, y_{avg}, was calculated using Eq. 16.

Figure 7a shows that the difference between the potential of the cell predicted by the DFM approach and by the CPM approach for a theoretical discharge rate of C/5 is very small. At a discharge rate of C/2 the differences become slightly bigger. Figure 7b shows that at high discharge rates the differences between the two approaches are very significant. This behavior is due to the lithium ion-lithium ion interactions inside the particle. The higher the discharge rates the larger the effect of the solid diffusion limitations in the performance of the cell, see Eq. 13. The initial drop in the potential of the cell is very steep, and this is basically due to the shape of the open-circuit potential at low lithium intercalation fractions (see Fig. 2b). According to Fig. 7, the DFM underpredicts the capacity of the cell, the larger the utilization the larger the capacity. This can also be observed in Table V which shows the discharge times of the cell at different galvanostatic theoretical discharge rates. The shorter the required time to discharge the cell the lower the capacity of the cell. For instance, at a 2C discharge rate the discharge time of the cell predicted by the DFM is 27% shorter than the time predicted by the

Table IV. Model parameters.

Parameter	Value	Ref.
T_{amb}	298 K	Adjustable
ef	4	Adjustable
ϵ_1	0.35	Adjustable
ϵ_s	0.55	21
S	0.05 m^2	37
L_{Li} (Eq. A-6, for y_0 = 0.01)	4.1×10^{-5} m	Adjustable
L_s	25×10^{-6} m	37
L_1	125×10^{-6} m	37
$L_{c,1}$	9×10^{-6} m	37
L (Eq. A-5)	2×10^{-4} m	Adjustable
v_c (Eq. A-4)	1×10^{-5} m^3	Adjustable
h_c	65 mm	Adjustable
r_c	9 mm	Adjustable
S_e (Eq. A-7)	4.2×10^{-3} m^2	Adjustable
R_s	3.5×10^{-6} m	24
L_p	0.01 m	24
a (Eq. A-8)	3.7×10^5 m^2/m^3	Adjustable
a_1 (Eq. A-9)	5000 m^2/m^3	Adjustable
a_2 (Eq. A-10)	0.084 m^2/m^2	Adjustable
M_{Li}	6.987 mol/g	
K_{Li}	4.1×10^{-6} mol$^{0.5}$/s m$^{0.5}$	11
α	0.5	11
h	5 W/m^2 K	21
ρ_s	950 kg/m^3	37
ρ_1	2220 kg/m^3	39
$\rho_{c,1}$	8930 kg/m^3	39
ρ_{Li}	534 kg/m^3	39
ρ_{PC}	1200 kg/m^3	40
ρ (Eq. A-13)	1470 kg/m^3	Adjustable
$C_{p,PC}$ (J/kg K)	720	40
$C_{p,1}$ (J/kg K)	$8.875 + 0.378\ T$	39
$C_{p,Cu}$ (J/kg K)	$1.4 \times 10^{-6}\ T^3 - 1.6 \times 10^{-3}\ T^2 + 0.987\ T + 225$	39
$C_{p,Li}$ (J/kg K)	$3.72\ T + 2423.1$	39

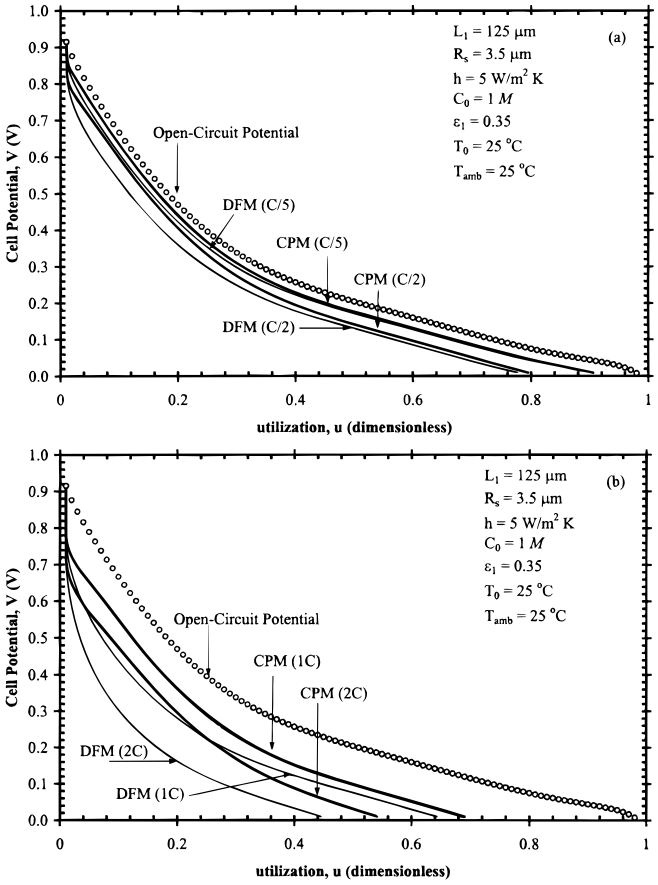

Figure 7. Cell potential *vs.* utilization of the cell at different galvanostatic theoretical discharge rates to 0.01 V cutoff voltage. (a) Low discharge rates. (b) High-medium discharge rates. The line of circles represents the open-circuit potential of the cell.

Table V. Discharge times of the cell at different galvanostatic theoretical discharge rates to 0.01 V cutoff potential.

Theoretical discharge rate	Time to discharge (min)	
	DFM	CPM
C/5 (12.05 A/m^2)	175.0	175.0
C/2 (30.12 A/m^2)	59.8	62.3
1C (60.23 A/m^2)	24.7	27.7
2C (120.46 A/m^2)	8.5	11.5

CPM. This means that the capacity of the cell predicted by the DFM is 27% smaller than the one predicted by the CPM approach. This was caused because the intercalation of lithium in the DFM approach was not corrected by the lithium ion interactions (activity coefficient term). In all the cases, the overall diffusion coefficient in the solid phase (that can be defined as the product of D_s by f_2) for the DFM is smaller than the overall diffusion coefficient for the solid phase used in the CPM (corrected by the lithium ion interaction).

Figure 8 shows the predicted temperature of the cell *vs*. the utilization for galvanostatic discharges at different theoretical discharge rates to a 0.01 V cutoff potential. At low discharge rates (C/5 and C/2) the temperature profile predicted by the DFM and CPM approaches are similar. At high discharge rates (1C and 2C), the temperature predicted by the DFM at a given utilization is significantly higher than the one predicted by the CPM (*i.e.*, at $u = 0.46$ the temperatures of the cell predicted at 2C are 57 and 53°C for the DFM and CPM, respectively). This is because the difference between the open-circuit potential and the potential of the cell ($U - V$) for the DFM is larger than for the CPM due to the solid diffusion limitations. Nevertheless, the maximum temperature predicted by the DFM is lower than the one predicted by the CPM at high discharge rates, because the capacity of the cell predicted by the CPM is higher than the one predicted by the DFM (allowing the cell to run for a longer period of time generating more ohmic heat). At low discharge rates (C/5 and C/2) the predicted temperature of the cell using both approaches (DFM and CPM) decreases at small utilization values as shown in Fig. 8 due to the effect of the entropy term (dU/dT). The entropy term can be obtained by taking the derivative of Eq. 9 respect to temperature

$$\frac{dU}{dT} = \frac{\Re}{F} \ln\left(\frac{1 - y|_{R=1}}{y|_{R=1}}\right) \quad \text{for } 0 < y|_{R=1} < 0.985 \qquad [33]$$

For the initial condition used ($y_0 = 0.01$) the entropy terms (dU/dT) predicted by both approaches (DFM and CPM) at the beginning of the discharge will be positive (see Eq. 33). At low discharge rates the solid diffusion limitations in the particle are not significant (as we show later). Therefore, the difference between the open-circuit potential and the potential of the cell ($U - V$) is not large enough with respect to the entropy term (dU/dT) causing the decrease of the temperature at the beginning of the discharge (small utilization values), see Eq. 27. At larger utilization values, the entropy terms become insignificant (and even get negative signs, see Eq. 33) with respect to the $U - V$ differences, increasing the temperature of the cell.

Figure 9 shows the lithium ion intercalation fraction inside a particle located at the separator/composite electrode interface ($x = 25$ μm) at different theoretical discharge rates, at short times in Fig. 9a ($t = 15$ s) and at long times in Fig. 9b ($t = 390$ s). The conditions of the simulations are given in Fig. 9a. As shown in Fig. 9a at low discharge rates (C/2) and short times the difference between the surface concentrations predicted by both approaches and the initial concentration (see Table III) is not large. This is because the cell is not solid-diffusion limited (this small change in the surface intercalation fraction causes the entropy effect in the temperature shown in Fig. 8). At high discharge rates (1C and 2C), the difference is more significant due to the solid diffusion limitations. Figure 9b shows the intercalation profile at long times. The higher the discharge rates the steeper the profiles of the lithium intercalation fraction and the higher the differences between the CPM and the DFM approaches. The intercalation of lithium ions inside the particle is faster with the CPM because the activity coefficient term will vary somewhere between 0.7 and 10 depending on the lithium ion fraction (most of the time about 1.0, see Fig. 2), while for the DFM the value is fixed in 1.0.

Figure 10 shows the lithium ion intercalation fraction at the particle surface in the carbon electrode for different galvanostatic theo-

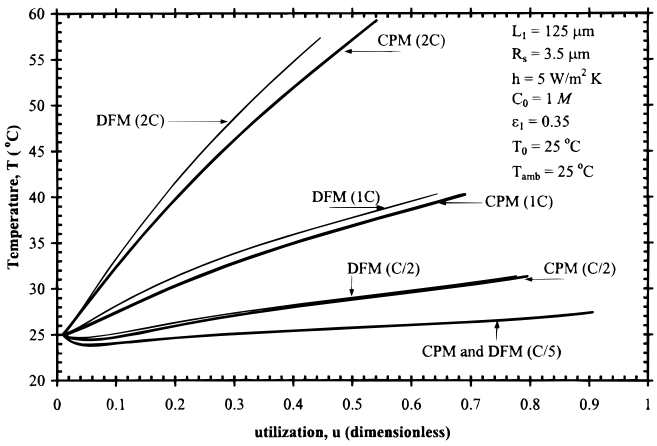

Figure 8. Cell temperature *vs*. utilization of the cell at different galvanostatic theoretical discharge rates to 0.01 V cutoff potential.

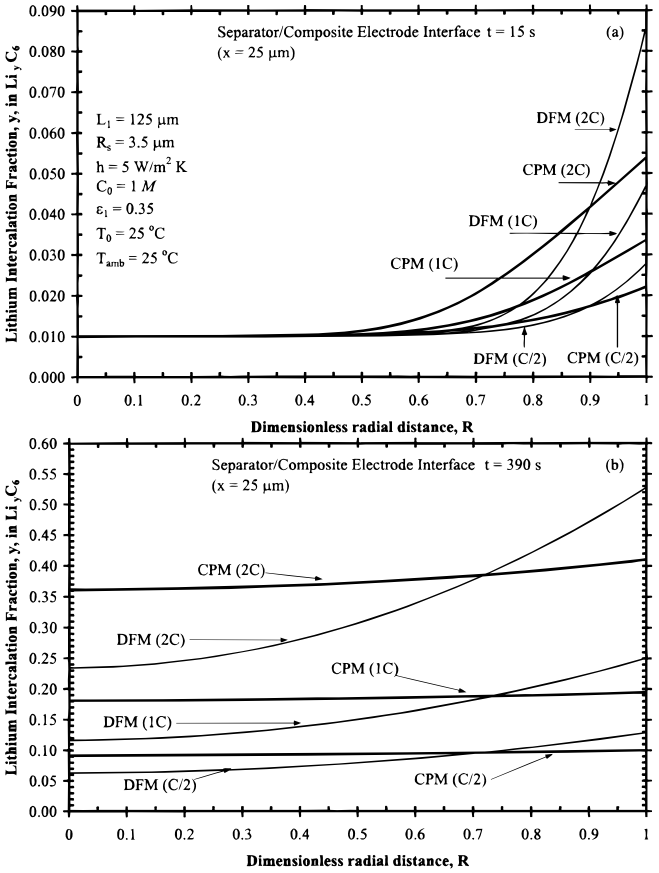

Figure 9. Lithium ion intercalation fraction inside a particle located at the separator/composite electrode interface. (a) Short time ($t = 15$ s). (b) Long time ($t = 390$ s).

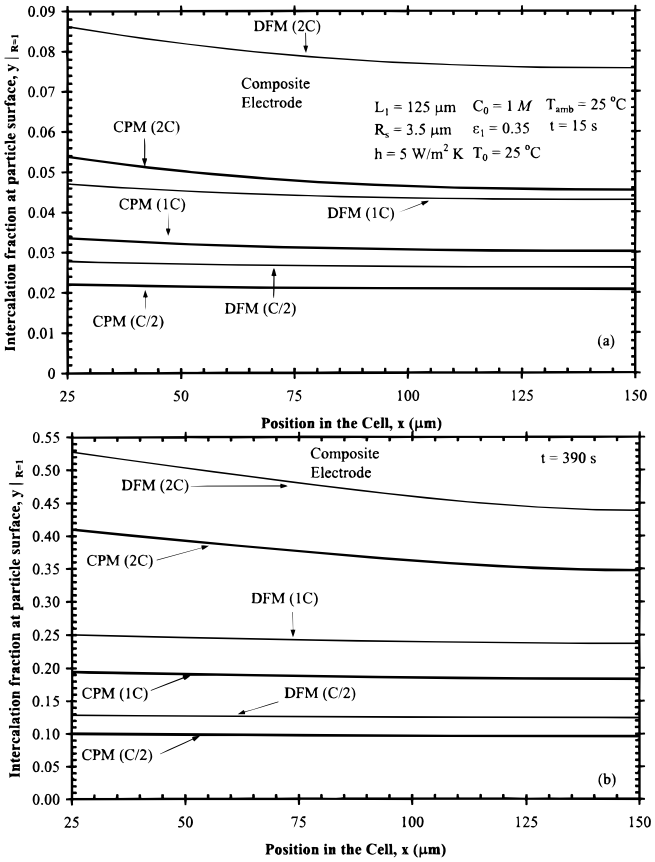

Figure 10. Intercalation fraction at the particle surface in the composite electrode. (a) Short times (t = 15 s). (b) Long times (t = 390 s).

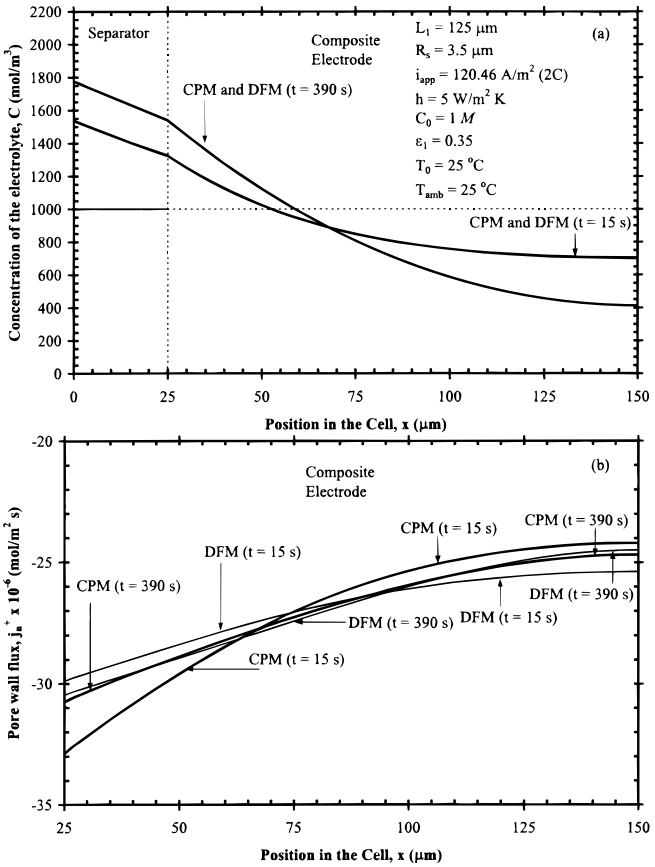

Figure 11. Electrolyte concentration profile and pore wall flux for a galvanostatic theoretical discharge rate of 2C at short (t = 15 s) and long times (t = 390 s). (a) Concentration of the electrolyte in the cell. (b) Pore wall flux in the composite electrode.

retical discharge rates at short and long times (Fig. 10a and b, respectively). The intercalation fraction at the particle surface decreases as the position inside the composite electrode (x) increases, because of the polarization of the electrolyte as we show later. The intercalation fraction at the surface predicted by the DFM is larger than the one predicted by the CPM, at short and long times (Fig. 10a and b, respectively). The effect is more significant at high discharge rates (1C and 2C). This behavior is caused because the solid diffusion limitations are stronger when using the DFM approach than when using the CPM approach as shown in Fig. 9.

Figure 11 shows the concentration profile and the pore wall flux in the cell at short and long times for a galvanostatic theoretical discharge rate of 2C. The conditions of the simulation are given in Fig. 11a. The concentration of electrolyte (given in Fig. 11a) at the back of the carbon fiber electrode decreases with increasing time as lithium is charged into the electrode. The polarization of the cell increases with time. There are no significant differences in the concentration of the electrolyte predicted by the two approaches at short and long times. This is because the differences in the pore wall flux predicted by the two approaches (DFM and CPM) are not significant enough (as shown in Fig. 11b) to cause strong changes in the concentration profile of the electrolyte (see Eq. 17). Figure 11b shows the pore wall flux in the composite electrode at short and long times. We can see that at long times there are no differences in the pore wall flux predicted by the two approaches. At long times the transport limitations in the electrolyte are more significant (see Fig. 11a). The high polarization of the electrolyte, and the ohmic overpotential will limit the cell. At short times there are some differences in the pore wall flux predicted by the two approaches. The polarization of the electrolyte at short times is low (see Fig. 11a), therefore the ohmic overpotential is not limiting the cell and the kinetic overpotential is important (see Eq. 10). Close to the separator (x = 25 μm) the pore wall flux predicted by the CPM is larger than the one predicted by the DFM, even tough the gradient of $\partial y/\partial R|_{R=1}$ predicted by the DFM is larger than the one predicted by the CPM (see Fig. 9b). This is because of the effect of the interaction term in the pore wall flux (see Eq. 4 and 6).

We have observed remarkable differences in the electrochemical and thermal performance of the cell predicted by the two approaches. As explained before most of the differences are due to the diffusion limitations in the solid phase. Equation 13 indicates that in order to reduce the diffusion limitations in the solid phase we need to decrease the applied current density, reduce the particle size of the electrode, increase the thickness of the electrode, and/or decrease the porosity of the electrode. If we want to keep the theoretical capacity of the cell constant the only change we can make to reduce the effect of the solid diffusion limitations is by decreasing the radius of the particle. Figure 12 shows the influence of the particle radius in the predictions of the two models. Figures 12a and b show the predicted potential and temperature of the cell, respectively. The size of the particle needs to be reduced to 1 μm to make the predictions from both approaches very similar. Thus for particle sizes lower than 1 μm the lithium ion-lithium ion interactions inside the particle become insignificant because the solid diffusion limitations in the cell has been reduced.

Conclusions

A comparison between the chemical potential model (CPM) and the diffusion model (DFM) for modeling the insertion process in a carbon porous electrode has been performed. The two different approaches were compared in some limiting and simplified cases, and in a lithium foil cell during galvanostatic discharge. In all the cases significant differences between the results predicted by the two models were observed.

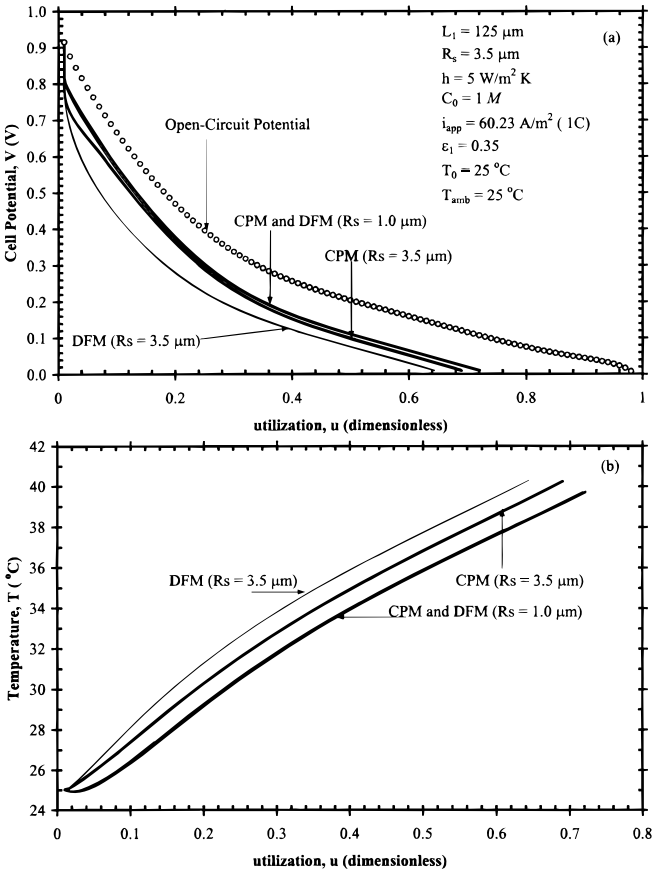

Figure 12. Effect of the particle size in the predictions of the two approaches for a 1 C galvanostatic theoretical discharge rate to 0.01 V cutoff voltage. (a) Predicted potential of the cell. (b) Predicted temperature of the cell.

Remarkable differences between the two approaches (DFM and CPM) were observed in a carbon fiber under potentiodynamic control. The results obtained by Verbrugge and Koch[24] were reproduced. Kinetic parameters obtained with the DFM may not represent the real kinetics of the system. One should not estimate exchange current densities (or reaction rate constants) and solid diffusion coefficients using the DFM. For the simplified case of the galvanostatic discharge of a cell under solid diffusion limitation, the DFM predicts steeper profiles for the lithium intercalation fraction inside the particle than the CPM.

The temperature of the cell predicted by the DFM is higher than the one predicted by the CPM at a given capacity. The discharge time of the cell predicted by the DFM is shorter than the one predicted by the CPM for medium-high discharge rates. The behavior is due to the lithium ion-lithium ion interactions. The lithium ion-lithium ion interactions are more significant when the cell is working under solid diffusion limitations. The radius of the particle needs to be very small for both approaches to predict similar results.

The results of the models indicate that the lithium ion-lithium ion interactions in the particle have a significant influence in the performance of the cell. Therefore, even though in all the cases the CPM requires more computational time than the DFM, the cell needs to be modeled using the CPM approach. That is, the performance of the cell should be modeled including the activity coefficient term in the solid phase, especially at high discharge rates.

The University of South Carolina assisted in meeting the publication costs of this article.

Appendix

Properties, Cell Parameters, and Density

The effective transport properties were obtained using Bruggeman correction which leads to[35]

$$D_{\text{eff,k}} = \epsilon_k^{1.5} D \quad [A\text{-}1]$$

$$\kappa_{\text{eff,k}} = \epsilon_k^{1.5} \kappa \quad [A\text{-}2]$$

where $k = 1$, s, and

$$\sigma_{\text{eff}} = \epsilon_1^{1.5} \sigma \quad [A\text{-}3]$$

The volume of the cell is calculated by

$$v_c = SL \quad [A\text{-}4]$$

where S is the projected surface area of the electrodes. S was fixed in 0.05 m^2. [21] The thickness of the cell (L) is given by

$$L = L_{\text{Li}} + L_s + L_1 + L_{c,1} \quad [A\text{-}5]$$

$L_{c,1}$ is the thickness of the carbon current collector. The thickness of the lithium foil electrode (L_{Li}) is calculated in order to balance the capacity of the carbon electrode. An additional amount of lithium foil (*ef*) is required to achieve a reasonable cycle life of the cell.[36] The thickness of the lithium foil is calculated by

$$L_{\text{Li}} = ef\, C_{s,\max}(1 - y_0)\epsilon_1 L_1 \frac{M_{\text{Li}}}{\rho_{\text{Li}} f_3} \quad [A\text{-}6]$$

where M_{Li} is the molecular weight of the lithium, ρ_{Li} represents the density of the lithium, and f_3 is a conversion factor equal to 1000 g/kg. The excess of lithium foil is usually between three to five times the amount required to balance the capacity of the composite material.[36] We assumed an excess of lithium foil of $ef = 4$.

The external surface area of the cell, S_e, is calculated by[21]

$$S_e = f_4 2\pi (r_c h_c + r_c^2) \quad [A\text{-}7]$$

We have used the dimensions of an 18,650 cell for the simulation, therefore, the radius and the height of the cell are $r_c = 9$ mm and $h_c = 65$ mm, respectively. f_4 is a conversion factor equal to 1×10^{-6} m^2/mm^2. The external surface area is given in square meters.

The interfacial area of solid-phase particles per unit volume of porous electrode, a, is given by

$$a = \frac{2(1 - \epsilon_1)}{R_s} \quad [A\text{-}8]$$

where the particles were assumed to be cylindrical.

The geometric electrode surface area per volume of the cell, a_1, is obtained by

$$a_1 = \frac{S}{v_c} \quad [A\text{-}9]$$

The ratio of external cell surface area to geometric electrode surface area, a_2, is given by

$$a_2 = \frac{S_e}{S} \quad [A\text{-}10]$$

The capacity of the cell is given by the theoretical capacity of the carbon electrode

$$C_{c,1} = \frac{C_{s,\max} F}{f_5 \rho_1} \quad [A\text{-}11]$$

where f_5 is a conversion factor equal to 3600 (A-g-s)/(mA-kg-h).

The applied current density equivalent to a theoretical 1C discharge rate (discharge of the cell in 1 h) is calculated based on the theoretical capacity of the carbon electrode as given

$$i_{\text{app}} = C_{c,1} L_1 \rho_1 f_6 \quad [A\text{-}12]$$

where f_6 is a conversion factor equal to 1 (A-g)/(mA-kg). The density of the carbon electrode, ρ_1, is defined for $y = 1$.

The density of the cell is calculated by an average of the components of the cell

$$\rho = \frac{\rho_s(1 - \epsilon_s)L_s + \rho_1(1 - \epsilon_1)L_1 + \rho_{c,1}L_{c,1} + \rho_{\text{Li}}L_{\text{Li}}}{L} \quad [A\text{-}13]$$

where ρ_s and $\rho_{c,1}$ are the densities of the separator and current collector of the carbon electrode, respectively. The current collector for the positive electrode

is copper.[37] The densities of the individual components of the cell are given in Table IV.

The heat capacity of the cell is obtained by an average of its components as shown below

$$C_p = \frac{C_{p,PC}\rho_{PC}(L_1\epsilon_1 + L_s\epsilon_s) + C_{p,1}\rho_1 L_1 + C_{p,Cu}\rho_{c,1}L_{c,1} + C_{p,Li}\rho_{Li}L_{Li}}{\rho_{PC}(L_1\epsilon_1 + L_s\epsilon_s) + \rho_1 L_1 + \rho_{c,1}L_{c,1} + \rho_{Li}L_{Li}} \quad [A\text{-}14]$$

where $C_{p,PC}$, $C_{p,1}$, $C_{p,Cu}$, and $C_{p,Li}$ are the heat capacities of propylene carbonate, carbon electrode, carbon current collector, and lithium, respectively. ρ_{PC} is the density of the solvent (propylene carbonate). The heat capacities of the individual components of the cell are given in Table IV. The heat capacity of the cell is a function of the temperature.

List of Symbols

a interfacial area of solid-phase particles per unit volume of porous electrode, m^2/m^3
a_1 geometric electrode surface area per unit volume of cell sandwich, m^2/m^3
a_2 ratio of external cell surface area to geometric electrode surface area, m^2/m^2
C concentration of the electrolyte, mol/m^3
$C_{c,1}$ theoretical capacity of the carbon electrode, (see Eq. A-11) mAh/g
C_p cell heat capacity, J/kg K
$C_{p,1}$ heat capacity of the carbon electrode, J/kg K
$C_{p,Cu}$ heat capacity of the carbon electrode current collector, J/kg K
$C_{p,Li}$ heat capacity of the lithium, J/kg K
$C_{p,PC}$ heat capacity of the propylene carbonate, J/kg K
C_s concentration of lithium in solid state, mol/m^3
$C_{s,max}$ maximum concentration of lithium in solid state, mol/m^3
D diffusion coefficient of the electrolyte, m^2/s
D_{eff} effective diffusion coefficient of the electrolyte, m^2/s
D_s diffusion coefficient of lithium in solid state when lithium concentration tends to zero, m^2/s
ef excess of lithium foil, (see Eq. A-6) dimensionless
f_1 conversion factor used in Eq. 11, 1×10^{-3} V/mV
f_2 interaction factor, dimensionless ($f_2 = 1$ DFM, $f_2 = 1 + d \ln \gamma_+/d \ln y$ CPM)
f_3 conversion factor used in Eq. A-6, 1000 g/kg
f_4 conversion factor used in Eq. A-7, 1×10^{-6} m^2/mm^2
f_5 conversion factor used in Eq. A-11, 3600 (A-g-s)/(mA-kg-h)
f_6 conversion factor used in Eq. A-12, 1 (A-g)/(mA-kg)
F Faraday's constant, 96,487 C/mol equiv
h heat transfer coefficient based on external cell surface area, W/m^2 K
h_c height of the battery, 65 mm
i current density at the surface of the particle, A/m^2
i_2 electrolyte phase current density, A/m^2
i_{app} applied current density, A/m^2
j_n^+ pore wall flux of Li^+ across particle-electrolyte interface, mol/m^2 s
k_a anodic rate constant,[24] mol/m^2 s (see Eq. 7)
k_c cathodic rate constant,[24] mol/m^2 s (see Eq. 7)
K reaction rate constant of the carbon fiber,[24] $mol^{0.5}/m^{0.5}$ s (see Eq. 10, $K = k_c^{1-\beta}k_a^{\beta}$)
K_{Li} reaction rate constant of the lithium foil electrode,[11] $mol^{0.5}/m^{0.5}$ s
L thickness of the cell, (see Eq. A-5) m
$L_{c,1}$ thickness of the carbon current collector,[37] m
L_k thickness of the particular region ($k = 1$ or s, see subscripts), m
L_{Li} thickness of the lithium foil, (see Eq. A-6) m
L_p length of the particle, m
M_{Li} molecular weight of lithium, 6.987 g/mol
nj number of nodes in the axial dimension of the cell (x), dimensionless
nr number of nodes in the radial direction, dimensionless
N_+ flux of lithium ions, mol/m^2 s
Q heat transfer rate from the cell to the environment per volume of the cell, W/m^3
r radial distance in the carbon fiber, m
r_c radius of the battery, 9 mm
R dimensionless radial distance in the carbon fiber, ($R = r/R_s$)
$\mathcal{R}$ universal gas constant, 8.314 J/mol K
R_s particle radius, m
S projected surface area of the electrodes,[21] (see Eq. A-4) m^2
S_c ratio of discharge time to the time constant for diffusion, (see Eq. 13) dimensionless
t time, s
t_+^0 transference number of lithium ions, dimensionless
T temperature of the cell, K
T_{amb} ambient temperature, K
v_c volume of the cell, (see Eq. A-4) m^3
V cell potential, V
u utilization of the cell defined by Eq. 32 , dimensionless
U open-circuit cell potential,[24] (see Eq. 9) V
U_{app} applied potential in the particle, V
U_0 initial potential in the particle, V
U_s standard open-circuit cell potential at infinitely dilute conditions,[24] V
x axial dimension in the cell, m
y dimensionless concentration of lithium ions in the solid carbon, ($y = C_s/C_{s,max}$) dimensionless
y_{avg} average lithium intercalation fraction inside the particle, (see Eq. 16) dimensionless

Greek

α transfer coefficient of lithium deposition-dissolution reaction,[11] dimensionless
β transfer coefficient of carbon fiber reaction,[24] dimensionless
γ_+ activity coefficient of lithium ions in the solid phase, dimensionless
δ lithium charge, dimensionless (see Eq. 7)
ΔR grid size in the radial dimension (see Fig. 6)
Δx grid size in the axial dimension (see Fig. 6)
ϵ_k porosity of the particular region ($k = 1$ or s, see subscripts), dimensionless
η surface overpotential, V
θ_s vacant site in the particle, dimensionless (see Eq. 7)
κ electrolyte ionic conductivity, S/m
κ_{eff} effective ionic conductivity, S/m
ρ density of the cell, kg/m^3
$\rho_{c,1}$ density of carbon electrode current collector, kg/m^3
ρ_{Li} density of lithium, 534 kg/m^3 (Ref. 39)
ρ_{PC} density of propylene carbonate, kg/m^3
ρ_s density of the separator, kg/m^3
σ electronic conductivity, S/m
σ_{eff} effective electronic conductivity of solid phase matrix, S/m
τ dimensionless time, ($\tau = tD_s/R_s^2$)
ν sweep rate, mV/s
ϕ_1 solid phase potential, V
ϕ_2 solution phase potential, V
Ω self-interaction coefficient of order k, J/mol

Subscripts

0 initial condition
k order of the series in Eq. 8 and 9, dimensionless
1 carbon electrode or solid phase
2 solution phase
s separator

References

1. G. G. Botte, V. R. Subramanian, and R. E. White, *Electrochim. Acta*, **45**, 2595 (2000).
2. S. Atlung, K. West, and T. Jacobsen, *J. Electrochem. Soc.*, **126**, 1311 (1979).
3. M. Doyle and J. Newman, *J. Appl. Electrochem.*, **27**, 846 (1997).
4. M. Doyle and J. Newman, *J. Power Sources*, **54**, 46 (1995).
5. S. Atlung, B. Zachau-Christiansen, K. West, and T. Jacobsen, *J. Electrochem. Soc.*, **131**, 1200 (1984).
6. R. Darling and J. Newman, *J. Electrochem. Soc.*, **144**, 3057 (1997).
7. T. F. Fuller, M. Doyle, and J. Newman, *J. Electrochem. Soc.*, **141**, 1 (1994).
8. T. F. Fuller, M. Doyle, and J. Newman, *J. Electrochem. Soc.*, **141**, 982 (1994).
9. K. West, T. Jacobsen, and S. Atlung, *J. Electrochem. Soc.*, **120**, 1480 (1982).
10. Z. Mao and R. E. White, *J. Power Sources*, **43/44**, 181 (1993).
11. M. Doyle, T. F. Fuller, and J. Newman, *J. Electrochem. Soc.*, **140**, 1526 (1993).
12. M. Doyle and J. Newman, *Electrochim. Acta*, **40**, 2191 (1995).
13. M. W. Verbrugge and B. J. Koch, *J. Electrochem. Soc.*, **143**, 24 (1996).
14. M. Doyle and J. Newman, *J. Electrochem. Soc.*, **143**, 1890 (1996).
15. R. Darling and J. Newman, *J. Electrochem. Soc.*, **144**, 4201 (1997).
16. G. S. Nagarajan, J. W. Van Zee, and R. M. Spotnitz, *J. Electrochem. Soc.*, **145**, 771 (1998).
17. R. Darling and J. Newman, *J. Electrochem. Soc.*, **145**, 990 (1998).
18. P. Arora, M. Doyle, A. S. Gozdz, R. E. White, and J. Newman, in *Advances in Mathematical Modeling and Simulation of Electrochemical Processes and Oxygen Depolarized Cathodes and Activated Cathodes for Chlor-Alkali and Chlorate Proccesses*, J. W. Van Zee, T. F. Fuller, P. C. Foller, and F. Hine, Editors, PV 98-10, p. 29, The Electrochemical Society Proceedings Series, Pennington, NJ (1998).
19. C. R. Pals and J. Newman, *J. Electrochem. Soc.*, **142**, 3274 (1995).
20. C. R. Pals and J. Newman, *J. Electrochem. Soc.*, **142**, 3282 (1995).
21. G. G. Botte, B. A. Johnson, and R. E. White, *J. Electrochem. Soc.*, **146**, 914 (1999).
22. M. Morita, N. Hishimura, and Y. Matsuda, *Electrochim. Acta*, **38**, 1721 (1993).
23. D. Guyomard and J. M. Tarascon, *J. Electrochem. Soc.*, **139**, 937 (1992).
24. M. W. Verbrugge and B. J. Koch, *J. Electrochem. Soc.*, **143**, 600 (1996).
25. M. Doyle, Ph.D. Thesis, University of California, Berkeley, CA (1995).

26. P. Arora, R. E. White, and M. Doyle, *J. Electrochem. Soc.*, **145**, 3647 (1998).
27. P. Arora, M. Doyle, and R. E. White, *J. Electrochem. Soc.*, **146**, 3543 (1999).
28. J. S. Newman, *Electrochemical Systems*, Prentice Hall, Inc., Englewood Cliffs, NJ (1991).
29. R. Kanno, Y. Kawamoto, Y. Takeda, S. Ohashi, N. Imanishi, and O. Yamamoto, *J. Electrochem. Soc.*, **139**, 3397 (1992).
30. D. Zhang, B. N. Popov, and R. E. White, *J. Electrochem. Soc.*, **147**, 831 (2000).
31. T. V. Nguyen and R. E. White, *Comp. Chem. Eng.*, **11**, 543 (1987).
32. S. Patankar, *Numerical Heat Transfer and Fluid Flow*, p. 31, Hemisphere Publishing Corporation, New York (1980).
33. D. A. Curtis, T. I. Evans, and R. E. White, *J. Electrochem. Soc.*, **136**, 3392 (1989).
34. G. G. Botte and R. E. White, Unpublished program (available upon request).
35. D. A. G. Bruggeman, *Ann. Phys.*, **24**, 636 (1935).
36. S. Hossain, in *Handbook of Batteries*, D. Linden, Editor, McGraw-Hill, Inc., New York (1995).
37. B. A. Johnson and R. E. White, *J. Power Sources*, **70**, 48 (1998).
38. J. M. Sullivan, D. C. Hanson, and R. Keller, *J. Electrochem. Soc.*, **117**, 779 (1970).
39. *CRC Handbook of Chemistry and Physics*, D. R. Lide, Editor, CRC Press, New York (1999).
40. M. W. Verbrugge, *AIChE J.*, **41**, 1550 (1995).